JCI The Journal of Clinical Investigation

Severe myopathy in mice lacking the MEF2/SRF-dependent gene leiomodin-3

Bercin K. Cenik, … , Eric N. Olson, Ning Liu

J Clin Invest. 2015;125(4):1569-1578. https://doi.org/10.1172/JCI80115.

Research Article **Muscle biology**

Maintenance of skeletal muscle structure and function requires a precise stoichiometry of sarcomeric proteins for proper assembly of the contractile apparatus. Absence of components of the sarcomeric thin filaments causes nemaline myopathy, a lethal congenital muscle disorder associated with aberrant myofiber structure and contractility. Previously, we reported that deficiency of the kelch-like family member 40 (KLHL40) in mice results in nemaline myopathy and destabilization of leiomodin-3 (LMOD3). LMOD3 belongs to a family of tropomodulin-related proteins that promote actin nucleation. Here, we show that deficiency of LMOD3 in mice causes nemaline myopathy. In skeletal muscle, transcription of *Lmod3* was controlled by the transcription factors SRF and MEF2. Myocardin-related transcription factors (MRTFs), which function as SRF coactivators, serve as sensors of actin polymerization and are sequestered in the cytoplasm by actin monomers. Conversely, conditions that favor actin polymerization de-repress MRTFs and activate SRF-dependent genes. We demonstrated that the actin nucleator LMOD3, together with its stabilizing partner KLHL40, enhances MRTF-SRF activity. In turn, SRF cooperated with MEF2 to sustain the expression of LMOD3 and other components of the contractile apparatus, thereby establishing a regulatory circuit to maintain skeletal muscle function. These findings provide insight into the molecular basis of the sarcomere assembly and muscle dysfunction associated with nemaline myopathy.

Severe myopathy in mice lacking the MEF2/SRF-dependent gene leiomodin-3

Bercin K. Cenik,[1] Ankit Garg,[1] John R. McAnally,[1] John M. Shelton,[2,3] James A. Richardson,[2,3] Rhonda Bassel-Duby,[1,4] Eric N. Olson,[1,4] and Ning Liu[1,4]

[1]Department of Molecular Biology, [2]Department of Pathology, [3]Department of Internal Medicine, and [4]The Hamon Center for Regenerative Science and Medicine, University of Texas Southwestern Medical Center, Dallas, Texas, USA.

Maintenance of skeletal muscle structure and function requires a precise stoichiometry of sarcomeric proteins for proper assembly of the contractile apparatus. Absence of components of the sarcomeric thin filaments causes nemaline myopathy, a lethal congenital muscle disorder associated with aberrant myofiber structure and contractility. Previously, we reported that deficiency of the kelch-like family member 40 (KLHL40) in mice results in nemaline myopathy and destabilization of leiomodin-3 (LMOD3). LMOD3 belongs to a family of tropomodulin-related proteins that promote actin nucleation. Here, we show that deficiency of LMOD3 in mice causes nemaline myopathy. In skeletal muscle, transcription of *Lmod3* was controlled by the transcription factors SRF and MEF2. Myocardin-related transcription factors (MRTFs), which function as SRF coactivators, serve as sensors of actin polymerization and are sequestered in the cytoplasm by actin monomers. Conversely, conditions that favor actin polymerization de-repress MRTFs and activate SRF-dependent genes. We demonstrated that the actin nucleator LMOD3, together with its stabilizing partner KLHL40, enhances MRTF-SRF activity. In turn, SRF cooperated with MEF2 to sustain the expression of LMOD3 and other components of the contractile apparatus, thereby establishing a regulatory circuit to maintain skeletal muscle function. These findings provide insight into the molecular basis of the sarcomere assembly and muscle dysfunction associated with nemaline myopathy.

Introduction

Contractility of striated muscle depends on the assembly of myriad proteins into the contractile apparatus of the sarcomere. Aberrant expression or mutations of sarcomeric proteins cause a variety of skeletal muscle diseases. Among these, nemaline myopathy, which results from mutations in thin-filament proteins, is associated with disorganization of myofibrils, reduced contractile force, mitochondrial dysfunction, and consequent failure to thrive. This form of myopathy is characterized by electron-dense "nemaline" bodies formed by the abnormal aggregation of proteins within myofibers (1–5). To date, mutations in 9 different genes encoding components of skeletal muscle actin thin filaments have been shown to cause nemaline myopathy (2, 4).

Recently, we showed that loss of function of the kelch domain protein KLHL40 in mice causes nemaline myopathy similar to that seen in human patients with KLHL40 mutations (6–9). Analysis of the proteome of skeletal muscle from *Klhl40*-mutant mice revealed pronounced downregulation of leiomodin-3 (LMOD3), a putative actin-nucleating protein that had not been previously studied (6). Subsequently, frame-shift and nonsense mutations in *LMOD3* were found to cause nemaline myopathy in humans, and inhibition of Lmod3 in zebrafish and *Xenopus* through morpholino-mediated knockdown was shown to cause myofiber disarray (10, 11).

LMOD3 belongs to a recently described family of tropomodulin-related proteins known as leiomodins that share a common domain organization comprising 3 predicted actin-binding domains and a tropomyosin-binding domain. Like tropomodulins, LMOD proteins bind to the pointed ends of actin filaments and promote actin polymerization by stabilizing binucleated or trinucleated actin via 3 actin-binding domains (12–16).

Actin dynamics are integrated with a transcriptional circuit involving myocardin-related transcription factors (MRTFs), which serve as coactivators of serum response factor (SRF) (17–19). G-actin monomers bind MRTFs, sequestering them in the cytoplasm, whereas actin polymerization releases MRTFs to enter the nucleus and coactivate SRF-dependent genes, including genes encoding actin and other components of the cytoskeleton and sarcomere (20, 21). This regulatory circuit thus allows for precise titration of actin expression in response to pathways that control cellular contractility and function. The MRTF/SRF pathway cooperates with the MEF2 transcription factors to regulate overlapping and distinct sets of muscle-specific contractile protein genes required for muscle function (19, 22–24).

In the present study, we investigated the function and regulation of LMOD3 in mice. We show that loss of function of LMOD3 causes lethal nemaline myopathy and severe disruption of skeletal muscle sarcomeric structure and function. Our results also show that MRTF/SRF and MEF2 directly regulate LMOD3 expression during skeletal muscle development, thereby providing a feed-forward circuit to coordinate the expression of LMOD3 with sarcomeric assembly. These findings provide important new insights into the molecular etiology of nemaline myopathy and suggest therapeutic strategies for enhancing sarcomeric function during the course of this disease.

Conflict of interest: The authors have declared that no conflict of interest exists.
Submitted: November 20, 2014; **Accepted:** January 29, 2015.
Reference information: *J Clin Invest*. 2015;125(4):1569–1578. doi:10.1172/JCI80115.

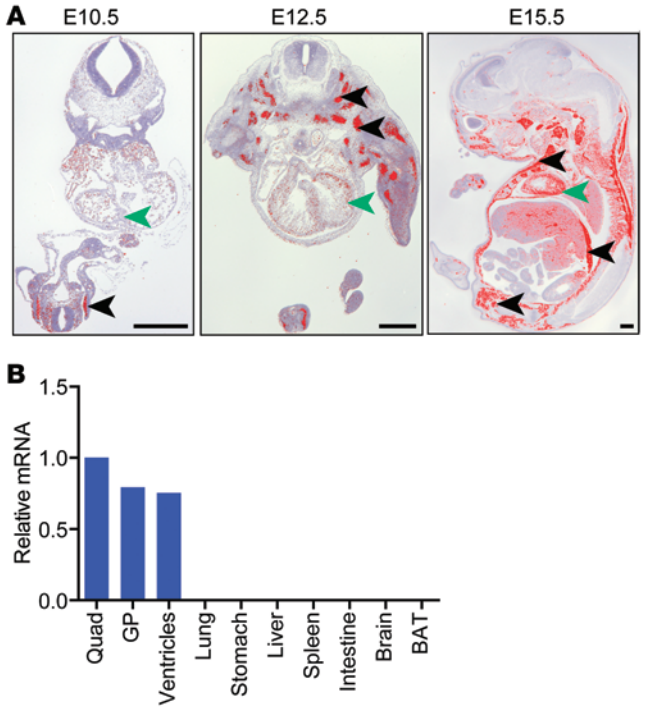

Figure 1. *Lmod3* is expressed selectively in the skeletal muscle and heart. (**A**) ISH analysis was performed on transverse sections of E10.5 and E12.5 embryos and sagittal sections of E15.5 embryos using radioisotopic antisense RNA probes against *Lmod3*. Black arrowheads denote developing muscle in E10.5 and E12.5 sections and intercostal muscles, diaphragm, and developing muscle groups in the limb bud in the E15.5 section. Green arrowheads indicate the heart. Scale bars: 500 μm. (**B**) qPCR analysis of *Lmod3* in an adult mouse shows heart- and muscle-specific expression. Experiments were performed in triplicate, and expression was normalized to 18S rRNA. Quad, quadriceps; GP, gastrocnemius and plantaris; BAT, brown adipose tissue.

Results

Muscle-specific expression of LMOD3. We surmised that LMOD3 would display a muscle-specific expression pattern similar to that of its binding partner KLHL40 (6). In situ hybridization (ISH) showed that *Lmod3* expression started as early as E10.5 in the myotome, the origin of skeletal muscle, whereas expression of *Lmod3* in the heart was not apparent until E12.5 (Figure 1A). By E15.5, robust expression of *Lmod3* was observed in both skeletal muscle and heart (Figure 1A), and this expression was maintained throughout adulthood (Supplemental Figure 1; supplemental material available online with this article; doi:10.1172/JCI80115DS1). Quantitative PCR (qPCR) and Northern blot analysis of adult tissues confirmed that *Lmod3* was specifically expressed in skeletal muscle and heart (Figure 1B and Supplemental Figure 1, A and B). Finally, Western blot analysis of LMOD3 in adult mice confirmed the skeletal muscle and heart-specific expression of LMOD3, with very scant expression in smooth muscle tissue (Supplemental Figure 1C). Enrichment of LMOD3 expression at the protein level was observed in soleus and diaphragm (Supplemental Figure 1C).

Generation of Lmod3-null mice by TALEN mutagenesis. To investigate the function of LMOD3 in vivo, we inactivated the gene using a TALEN mutagenesis strategy (Figure 2A). TALEN pairs targeting the second exon of *Lmod3* were designed, leading to a premature termination codon after codon 133, thereby removing the leucine-rich repeat and WH2 actin–binding domains (Figure 2A and Supplemental Figure 2, A and B). Cleavage activity of TALENs was confirmed by an in vitro cleavage assay (Supplemental Figure 2C). Two separate lines of mice were generated (with 2 and 10 nucleotide frameshift deletions, hereafter referred to as Δ2- and Δ10-KO mice, respectively), and loss of *Lmod3* mRNA and protein was confirmed in the heart and skeletal muscle tissue of these animals (Figure 2, B and C, and Supplemental Figure 1A). To eliminate the possibility of off-target effects of TALEN mutagenesis, we confirmed that the Δ10-KO mice recapitulated the phenotype of the Δ2-KO line in all our experiments. The results in this study focus primarily on the Δ2-KO mouse line.

Loss of LMOD3 results in a failure-to-thrive phenotype. *Lmod3*-KO mice were born at Mendelian ratios from heterozygous intercrosses and were indistinguishable from their WT littermates at birth. However, *Lmod3*-KO mice gradually displayed a failure-to-thrive

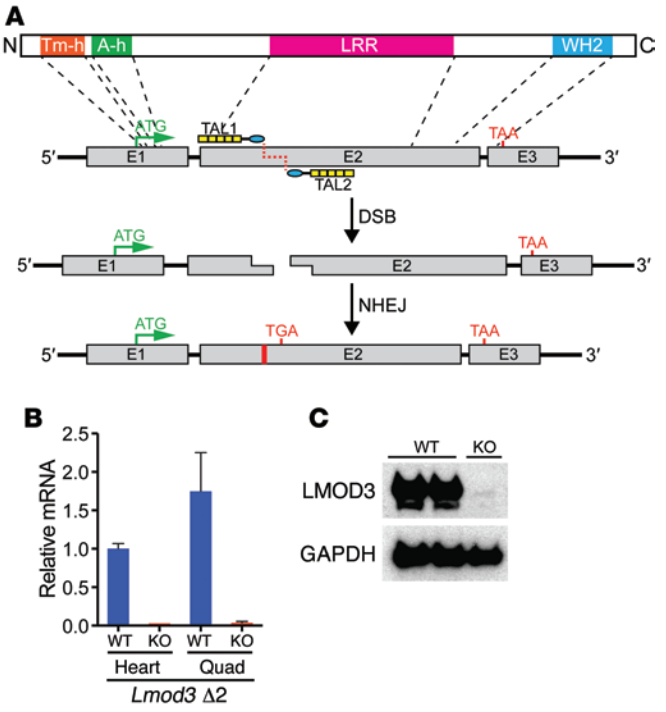

Figure 2. TALEN-induced frameshift mutagenesis eliminates LMOD3 at the RNA and protein levels. (**A**) LMOD3 protein structure, intron-exon structure of the *Lmod3* gene, and gene-targeting strategy. TALEN pairs targeting the second exon induce double-stranded breaks (DSB), followed by error-prone nonhomologous end-joining (NHEJ) repair. Frameshift deletions lead to premature termination of transcription. LRR, leucine-rich repeat; Tm-h, Tm-binding helix; A-h, actin-binding helix; WH2, Wiskott-Aldrich syndrome protein homology domain 2. (**B**) Loss of *Lmod3* mRNA was confirmed in the heart and quadriceps of KO mice and in those of their control WT littermates (n = 3/group). Experiments were performed in triplicate, and expression was normalized to 18S rRNA. (**C**) Western blot analysis of skeletal muscle with an antibody recognizing the N-terminal of LMOD3 protein showed a complete loss of LMOD3 in KO mice. GAPDH was used as a loading control.

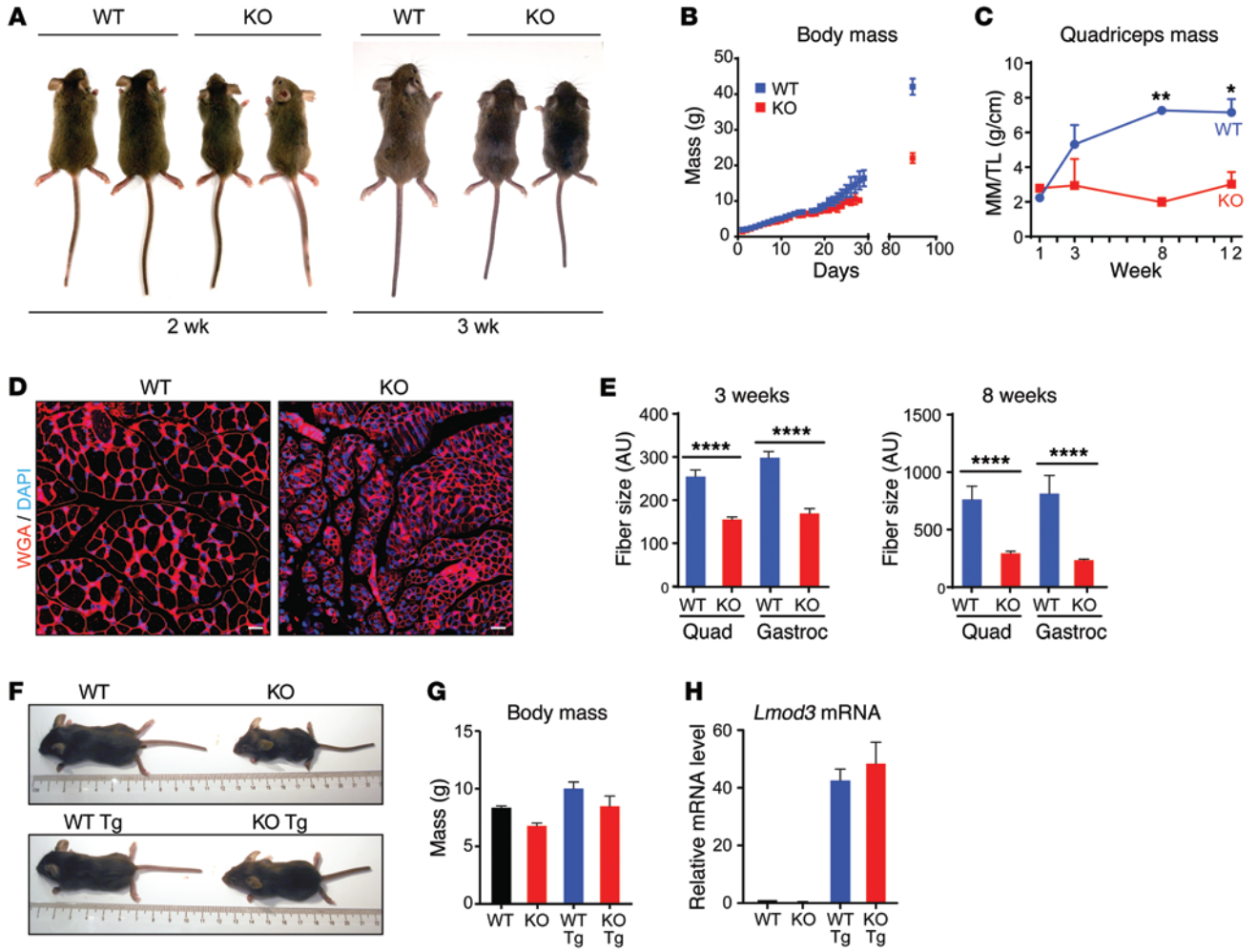

Figure 3. *Lmod3*-KO mice have a failure-to-thrive phenotype, which is rescued by the *MCK-Lmod3* transgene. (**A**) Photos of 2- and 3-week-old *Lmod3*-KO mice with sex-matched WT littermates show significant size differences. (**B**) Growth curve of KO male mice and WT male littermates shows failure to thrive in the KO mice. (**C**) A significant difference in muscle mass was observed in the KO mice compared with that of their WT littermates ($n \geq 10$ animals per group). $^{**}P < 0.01$; $^{*}P < 0.05$. MM/TL, muscle mass/tibia length. (**D**) Wheat-germ agglutinin (WGA) staining of muscle membranes in quadriceps of P12 mice showed reduced myofiber size in KO mice compared with that in WT littermates. WGA (red), DAPI (blue). Scale bars: 20 μm. (**E**) Quantification of myofiber area in quadriceps and gastrocnemius (Gastroc) muscles from transverse sections stained with laminin (shown in Figure 4B). Fiber size was calculated by particle analysis using ImageJ software. $^{****}P < 0.0001$. (**F**) Representative image of *MCK-Lmod3* Δ2-KO mice (KO Tg) and Δ2-KO mice, together with their *MCK-Lmod3* (WT Tg) and WT littermates showing complete rescue of the KO phenotype, with muscle-specific overexpression of LMOD3 with the *MCK-Lmod3* transgene. (**G**) Body mass of KO Tg mice was indistinguishable from the body mass of WT and WT Tg mice. WT, $n = 3$; WT Tg, $n = 3$; KO, $n = 3$; and KO Tg, $n = 3$. Animals were 3-week-old males. Data are presented as the mean ± SEM. (**H**) *Lmod3* expression in the skeletal muscle (gastrocnemius) of 3-week-old mice was assayed by qPCR. Experiments were performed in triplicate with 3 biological replicates, and expression was normalized to 18S rRNA.

phenotype, with the size difference between the KO mice and their WT littermates becoming more pronounced with age (Figure 3A). In order to ascertain that the failure to thrive was not due to difficulty in suckling or breathing, we confirmed that KO mice had milk spots comparable to those of their WT littermates. Furthermore, conventional histologic analysis showed that the diaphragms were unaffected (data not shown). The KO mice survived to adulthood, had the same lifespan as that of their WT littermates, and could breed successfully. However, they remained runted compared with their WT littermates (Figure 3B). The degree of runting varied between mice, likely due to the mixed background, and there were cases of extreme failure to thrive (Supplemental Figure 3). Both male and female mice displayed the same growth curves. Concurrent with the failure to thrive, muscle sizes and growth rates were also stunted, and hypoplastic myofibers were observed in the KO mice (Figure 3, C–E). The hearts of KO mice were also smaller starting from P7 and throughout adulthood (Supplemental Figure 4, A and B). Despite the smaller-sized hearts, cardiac function was minimally impaired in the KO animals (Supplemental Figure 4C), suggesting that loss of LMOD3 in skeletal muscle was primarily responsible for the failure-to-thrive phenotype.

To verify that the failure-to-thrive phenotype was caused by loss of LMOD3, as well as to eliminate possible off-target effects of TALEN mutagenesis, we generated Tg mice expressing LMOD3 under the control of the muscle-specific muscle creatine kinase (*MCK*) promoter (hereafter referred to as *MCK-Lmod3* Tg mice). *MCK-Lmod3* Tg mice were healthy and showed no pathology in the skeletal muscle or heart due to the overexpression of LMOD3

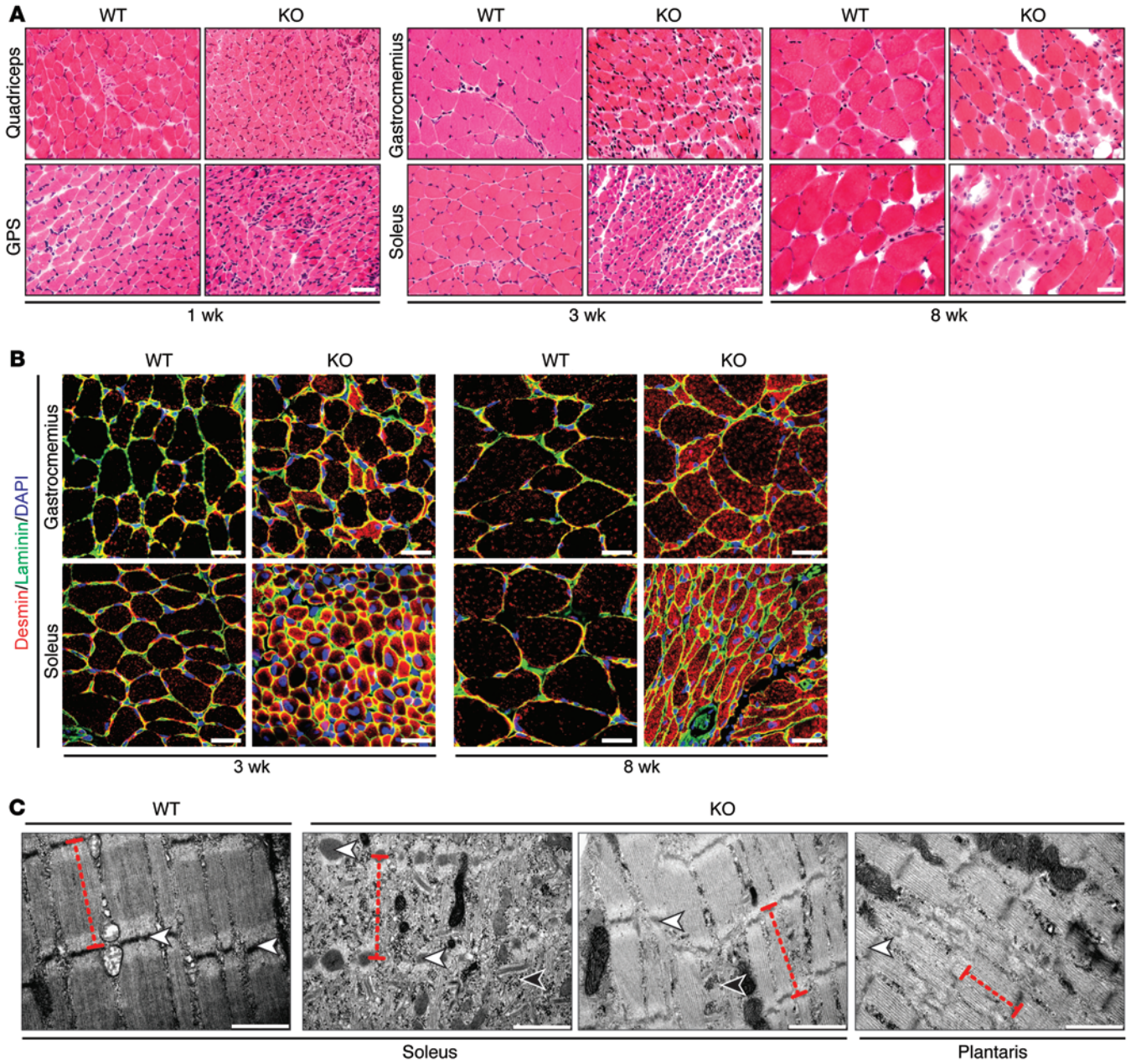

Figure 4. Loss of LMOD3 causes nemaline myopathy in mice. (**A**) H&E staining of quadriceps, gastrocnemius, plantaris, and soleus (GPS) muscles from 1-, 3- and 8-week-old WT and KO mice. By 3 weeks of age, centralization of nuclei and loss of sarcomeric organization were observed in the KO mice. Scale bars: 40 μm. (**B**) Desmin (red), laminin (green), and DAPI (blue) immunostaining of transverse myofibers shows centralized nuclei and pathological desmin accumulation in the KO muscle. Scale bars: 40 μm. (**C**) Transmission electron microscopic images of longitudinal sections of the soleus muscle from 3-week-old WT and KO mice showing loss of sarcomeric organization, increased glycogen accumulation, and replacement of sarcomeric Z lines by electron-dense nemaline bodies. Dotted lines indicate healthy sarcomere in WT muscle and demarcate disorganized sarcomeres in KO muscle. White arrowheads denote Z lines in WT muscle and mark the nemaline bodies (second panel) or Z-line streaming (third and fourth panels) in KO muscle. Black arrowhead denotes glycogen granules. All histologic analyses were performed in age- and sex-matched littermates (n = 3/group). Scale bars: 1 μm.

(data not shown). We crossed *MCK-Lmod3* Tg mice with Δ2-KO mice. Overexpression of LMOD3 was confirmed in both the WT and KO backgrounds. The *MCK-Lmod3* transgene was sufficient to rescue the failure-to-thrive phenotype of KO mice, as *Lmod3*-KO *MCK-Lmod3* Tg mice were indistinguishable from their WT littermates (Figure 3, F–H).

Deficiency of LMOD3 in skeletal muscle disrupts sarcomeric organization. To further characterize the muscle abnormalities of the *Lmod3*-KO mice, we performed histologic analyses of skeletal muscle samples at multiple time points. Reduced myofiber size was apparent as early as P7, and became more pronounced with age (Figure 4A). At 3 weeks of age, when mutant mice became visibly emaciated compared with their healthy WT littermates, centralization of myofiber nuclei (Figure 4A) and pathological desmin accumulation (Figure 4B) were observed. Furthermore, phalloidin staining of longitudinal muscle sections showed disorganization

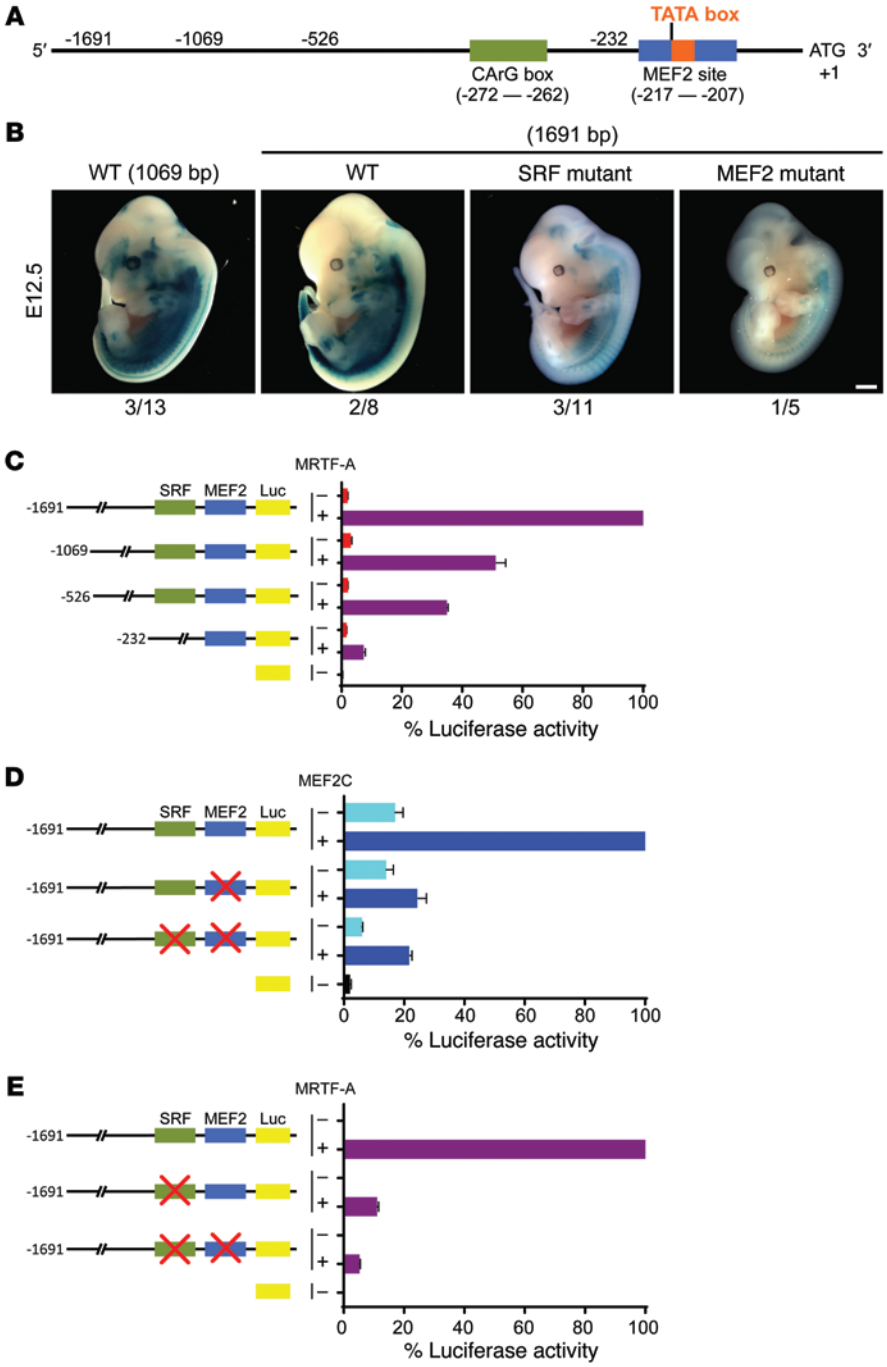

Figure 5. Regulation of *Lmod3* promoter by MEF2 and SRF transcription factors. (**A**) The *Lmod3* promoter region contains consensus sites for MEF2 and SRF (CArG box). The MEF2 site is also a TATA box. Numbering of nucleotide positions is relative to the ATG (+1) start codon. (**B**) LacZ staining was performed on E12.5 F_0 embryos containing the 1691- or 1069-bp enhancer fragment of the *Lmod3* promoter cloned into an *hsp68-LacZ* construct. WT *Lmod3* Tg embryos showed strong muscle-specific expression that was diminished in the SRF/MEF2 Tg mutants. Scale bar: 1 mm. (**C**) COS-7 cells were transfected with the upstream fragments of the *Lmod3* gene cloned into the luciferase reporter plasmid pGL3. Luciferase reporter assays showed activation of the *Lmod3* promoter by SRF in response to its coactivator MRTF-A. (**D**) Luciferase activity was measured in COS-7 cells transfected with the 1691-bp *Lmod3* reporter plasmid with or without mutations in the MEF2 site and/or the CArG box. Cells were cotransfected with MEF2C. (**E**) Luciferase reporter activity was measured in COS-7 cells transfected with the 1691-bp *Lmod3* reporter plasmid with or without mutations in the CArG box and/or the MEF2 site. Cells were cotransfected with MRTF-A. Experiments were performed at least twice, with all transfections done in triplicate. All results are reported as percentage values ± SEM (WT construct with MEF2C and MRTF-A was set to 100%). Luc, luciferase.

of sarcomeres and disruption of thin-filament architecture in the KO muscle tissue (Supplemental Figure 5). Sarcolipin, a marker of muscle disease, was robustly upregulated in the KO muscle (Supplemental Figure 6A). Centralized nuclei could be due to either myofiber degeneration and regeneration, or centronuclear myopathy. To further investigate the basis of the myofiber abnormalities, we performed Evans blue dye (EBD) leakage analysis and serum creatine kinase (CK) measurements. Serum CK was not elevated in KO mice, nor was there increased EBD penetration into the myofibers (data not shown). Furthermore, genetic markers of muscle atrophy and regeneration were not elevated (Supplemental Figure 6, B and C). Together, these findings ruled out myofiber degeneration and regeneration. Interestingly, the pathology was most dramatic in the soleus muscle, with the gastrocnemius and quadriceps muscles being affected to a lesser extent (Figure 4, A and B). This could be attributed to enrichment of LMOD3 expression in the soleus muscle at the protein level (Supplemental Figure 1C). In all cases, areas of muscle where sarcomeric organization was maintained were still present.

Electron microscopic analysis of the soleus muscles of 3-week-old mice revealed extensive disruption of sarcomeres in KO muscle compared with the organized architecture observed in the WT muscle, which consisted of parallel sarcomeres aligned vertically (Figure 4C). Most of the organized structure of the sarcomere was

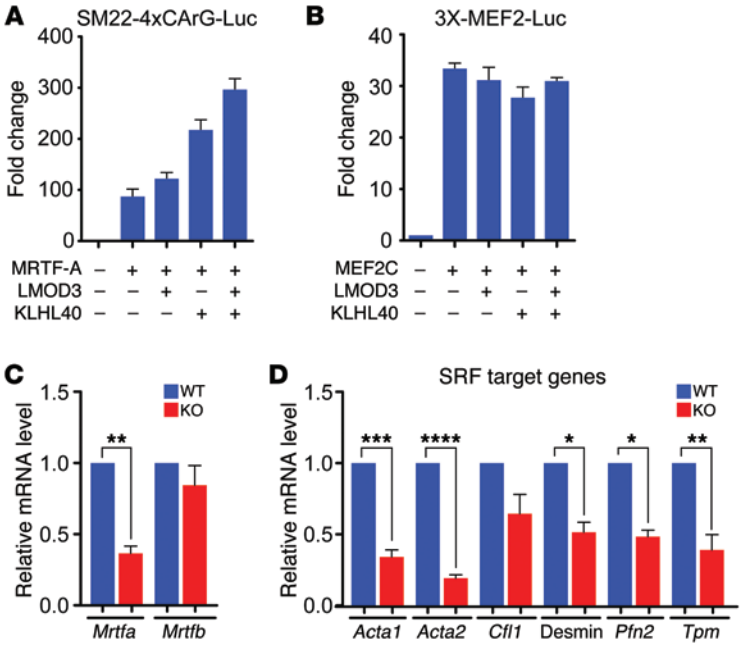

Figure 6. LMOD3 and KLHL40 regulation of MRTF/SRF and MEF2 pathways. Synthetic luciferase reporters with multimerized (**A**) CArG boxes (SM22-4x-CArG) and (**B**) MEF2 sites (3x-MEF2-Luc) were transfected into COS-7 cells, together with LMOD3 and/or KLHL40 expression vectors. Cells were cotransfected with MRTF-A (**A**) or MEF2C (**B**). Experiments were performed at least twice, with all transfections done in triplicate. All results are reported as fold change ± SEM. (**C** and **D**) qPCR analysis was performed on gastrocnemius muscles from WT and KO mice for (**C**) *Mrtf* gene expression and (**D**) SRF target gene expression. Experiments were performed in triplicate, and expression was normalized to 18S rRNA. $^{*}P < 0.05$; $^{**}P < 0.01$; $^{***}P < 0.001$; $^{****}P < 0.0001$.

replaced with remnants of sarcomeres consisting of irregular, disarrayed lamellae in the mutants, although areas where sarcomeric organization was relatively well preserved were also observed (Figure 4C, second and third panels). Additionally, the Z lines of the sarcomeres were replaced by nemaline bodies, which appeared as distinct rod-like inclusions (Figure 4C, second panel) (1, 25, 26). Accumulation of glycogen in the form of electron-dense granules, another feature of nemaline myopathy (1), was also apparent (Figure 4C, second through fourth panels).

Regulation of LMOD3 expression by MRTF/SRF and MEF2. Upon inspection of the *Lmod3* promoter, we discovered potential consensus sites for MEF2 (CTTAATATAG) and SRF [CC(A/T)$_6$GG] (CArG box) upstream of the start codon (Figure 5A). Interestingly, the MEF2 site was also superimposed on a TATA sequence, a phenomenon previously observed in other muscle genes (27, 28). These sites are conserved across vertebrate species (Supplemental Figure 7). Previously, ChIP assays showed that MEF2 and SRF occupied these sites in HL-1 cardiac muscle cells (29).

To determine whether the CArG box and MEF2 *cis*-regulatory elements were functional in vivo, we generated Tg mice with the 1.6- or 1.0-kb *Lmod3* promoter region fused to a *LacZ* reporter cassette (*hsp68-LacZ*) (30) and analyzed transgenic founder (F_0) embryos at E12.5 for β-galactosidase expression. Embryos harboring the 1.6- or 1.0-kb WT *Lmod3* promoter displayed a skeletal muscle–specific expression pattern of β-galactosidase, with prominent staining in the myotome and the developing muscles of the limb bud (Figure 5B). Mutations in both the CArG box and the MEF2-binding site greatly diminished β-galactosidase expression in vivo (Figure 5B, third and fourth panels). Furthermore, *Lmod3* (as well as *Lmod2* and *Klhl40*) mRNA expression was shown to be significantly downregulated in satellite cells isolated from mice carrying satellite cell–specific deletion of *Mef2a*, *Mef2c*, and *Mef2d* (*Pax7-Cre-ERT2 Mef2a$^{fl/fl}$ Mef2c$^{fl/fl}$ Mef2d$^{fl/fl}$*, hereafter referred to as MEF2-TKO mice; ref. 31), further demonstrating that LMOD3 is regulated by MEF2 (Supplemental Figure 8).

To test the functionality of the MEF2 and SRF sites, we performed luciferase reporter assays using the *Lmod3* promoter region in COS-7 cells. MRTF-A potently activated an *Lmod3* reporter containing a 1.6-kb fragment of the upstream region, suggesting SRF regulation of the *Lmod3* gene (Figure 5C). Indeed, a mutation of the CArG box (CCAAAAAGGG → C**A**AAAAA**C**G**C**) in the *Lmod3* promoter strongly diminished activation by MRTF-A (Figure 5E). Although truncation of the *Lmod3* promoter region progressively reduced its activity, significant activity, even with a 0.25-kb fragment, was evident (Figure 5C). This could be explained by the fact that, while the CArG box was not present in this smallest fragment, the MEF2 site was still intact. Cotransfection of the *Lmod3* reporter with MEF2C induced robust activation of the promoter linked to a luciferase reporter (~3-fold) (Figure 5D). In contrast, mutations in the MEF2 site that prevented binding (TTAATATAG → **CC**AATATAG) greatly diminished luciferase activity. In order to rule out the disruption of the TATA sequence as the cause of this loss of expression, we generated a construct that abolished MEF2 binding without disrupting the TATA box, as well as a construct with point mutations inside the TATA box. Both mutated constructs caused an approximate 4-fold decrease in luciferase activity; data are shown for the construct with the intact TATA box (Figure 5D). Combined mutations of the SRF and MEF2 sites in the *Lmod3* promoter diminished luciferase activity even further (Figure 5, D and E).

Modulation of the MRTF/SRF and MEF2 pathways by KLHL40/LMOD3. Given the importance of actin cycling in the control of MRTF activity (17, 19) and the role of KLHL40 in the stabilization of LMOD3 (6), which controls actin nucleation (10), we hypothesized that LMOD3 and KLHL40 influence the MRTF/SRF and MEF2 pathways by regulating actin cycling. To test this hypothesis, we conducted luciferase reporter assays with synthetic SM22-4xCArG and 3X-MEF2 luciferase promoters, which show robust activation in response to MRTF-A and MEF2C, respectively (18, 32). LMOD3 alone did not activate the 4xCArG pro-

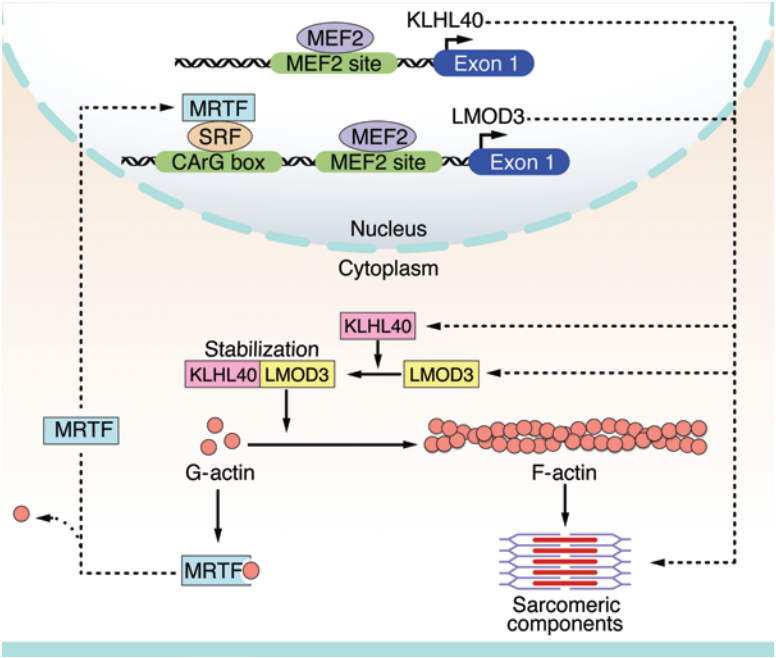

Figure 7. A model for the role of LMOD3 and KLHL40 in actin cycling and MRTF/SRF- and MEF2-dependent transcription. In normal muscle cells, MRTF/SRF and MEF2 regulate LMOD3 expression, and MEF2 regulates KLHL40 expression. KLHL40 functions in the cytoplasm to stabilize LMOD3 protein. Together, they promote actin polymerization by converting G-actin to F-actin, allowing normal sarcomeric function. In muscles lacking LMOD3, accumulation of G-actin monomers not only disrupt sarcomeric integrity, but also repress MRTF-A expression, which in turn suppresses SRF-dependent target genes encoding cytoskeletal proteins and components of the contractile apparatus, leading to nemaline myopathy.

moter, which was not unexpected, since LMOD3 is unstable in the absence of KLHL40 (6). KLHL40 alone induced a 2-fold increase in reporter gene expression, and when coexpressed with LMOD3, the promoter showed further activation (Figure 6A). On the other hand, there was no increase in activity of the 3X-MEF2-luciferase reporter with the addition of KLHL40, with or without LMOD3 (Figure 6B), pointing to a selective effect of KLHL40/LMOD3 signaling on the MRTF/SRF axis. We found that *Mrtfa* itself was also downregulated in *Lmod3*-KO mice (Figure 6C), suggesting the existence of a positive feedback loop to amplify MRTF-A expression. SRF target genes, which include those encoding for cytoskeletal proteins and the contractile apparatus, were also significantly downregulated in KO muscles (Figure 6D).

Discussion

The present study identifies the muscle-specific gene *Lmod3* as the causative gene for a nemaline-like congenital myopathy in mice. In the presence of KLHL40, the actin-binding function of LMOD3 enhances the activity of MRTF transcription factors, which coactivate SRF. In a complementary aspect of this circuitry, SRF, together with MEF2, controls the expression of LMOD3 and other cytoskeletal components in order to maintain skeletal muscle function (Figure 7). While this work was being completed, a supporting report was published, describing loss-of-function mutations of LMOD3 in human patients with nemaline myopathy (10). Morpholino-mediated knockdown of Lmod3 in zebrafish was also shown to cause myofiber disruption (10). Together, these studies uncover a critical role for LMOD3 in the maintenance of skeletal muscle structure and function.

Loss of LMOD3 in the skeletal muscle causes nemaline myopathy. Nemaline myopathy is a disease of the sarcomeric thin filaments. Recently, we showed that loss of KLHL40 in mice causes nemaline myopathy (6). Under normal conditions, KLHL40 maintains the expression of nebulin, another protein implicated in nemaline myopathy, and LMOD3 in the sarcomere, thus stabilizing the thin filament (6). Skeletal muscle from *Lmod3*-KO mice showed a marked disruption of sarcomeric organization by conventional histology, whereas sarcomeric disorganization in *Klhl40*-KO skeletal muscle was comparatively mild at the histological level and only detectable by electron microscopy. Skeletal muscle from *Lmod3*-KO mice also displays abnormal glycogen accumulation and nemaline rods, which appear as electron-dense inclusions attributed to the accumulation of disarrayed Z-line proteins, a hallmark of nemaline myopathy (2, 33).

LMOD3 and KLHL40 modulate MRTF/SRF and MEF2 transcriptional pathways to maintain sarcomeric integrity. Muscle integrity is dependent upon the maintenance of sarcomeric proteins, most notably actin. Actin exists in 2 forms inside the cell: globular monomeric G-actin and filamentous F-actin, which forms the thin filament of the sarcomere. The cycling of actin between these 2 forms is precisely regulated at the transcriptional and translational levels. The MRTF/SRF transcriptional circuit plays a key role in modulating actin cycling in the cell (19). We showed previously that KLHL40 expression is downregulated in skeletal muscle of MEF2-TKO mice, thus demonstrating that *Klhl40* is a MEF2-dependent gene (31). Here, we show that LMOD3 and LMOD2 show similar dependence on MEF2 for expression.

As schematized in Figure 7, the ability of LMOD3 to promote actin polymerization allows for the fulfillment of a feed-forward regulatory circuit to control the transcription of genes encoding sarcomeric components including LMOD3 itself. The *Lmod3* gene, like many other sarcomeric protein genes, is directly regulated by SRF, which in turn is controlled by members of the MRTF family. These potent coactivators cycle between the cytoplasm and the nucleus in response to changes in actin dynamics. In the presence of depolymerized G-actin, MRTFs are sequestered in the cytoplasm, preventing activation of SRF and their target genes. Conversely, stimuli that promote actin polymerization diminish

the pool of G-actin, freeing MRTFs to stimulate SRF activity, generating further sarcomeric components. Thus, LMOD3, by promoting actin polymerization, diminishes G-actin levels and drives its own expression through an amplification mechanism involving SRF as the intermediary. Consistent with this model, we show that LMOD3 activates the SM22-4xCArG reporter, which is highly sensitive to SRF. This model predicts that other CArG box–dependent genes would also be downregulated in *Lmod3*-mutant mice, which was indeed the case in our study. By stabilizing LMOD3, KLHL40 can also stimulate the expression of LMOD3 and other sarcomeric components. In addition, our results reveal a synergistic role for MEF2 in the activation of LMOD3 expression.

Actin polymerization is also subject to precise control by several actin-binding proteins that govern assembly of actin polymers at the pointed end and depolymerization at the barbed end, maintaining constant actin turnover. Formation of dimers and trimers from monomeric actin is the least energetically favorable, and therefore rate-limiting, step of actin polymerization. In order to overcome this barrier, cells use several actin-nucleating factors that directly nucleate actin monomers (reviewed in ref. 12).

LMOD proteins belong to the WH2 family of actin nucleators, which are recognized by the presence of 3 or more actin-binding domains (34, 35). While the exact mechanism by which WH2 domain proteins nucleate actin is unknown, current models support the idea that these proteins stabilize actin monomers in the trimer conformation, thus promoting nucleation. For instance, spire, a versatile actin nucleator, promotes nucleation by cooperative binding of each WH2 domain to actin without allowing it to dissociate (36). Similarly, it has been shown that LMOD2 binds actin to promote nucleation by stabilizing the actin trimer at the pointed end of the filament (13). The actin nucleation property of LMOD3 has recently been demonstrated in vitro by actin polymerization assays (10).

Nuclear G-actin also plays an important role in regulating the MRTF/SRF pathway. Binding of G-actin to MRTF in the nucleus enables MRTF export to the cytosol (21). Yuen et al. recently showed that LMOD3 shows a granular cytoplasmic staining pattern (10). Therefore, it is possible that this facet of SRF regulation functions independently of LMOD3, and re-sequestration of MRTF by G-actin in the cytoplasm prevents a sharp increase in SRF signaling.

We previously performed localization studies with EGFP-tagged LMOD3 and KLHL40 (6) using second harmonic generation (as described in ref. 37). These studies showed that LMOD3 localizes to the A band in both contracted and relaxed muscle. KLHL40 also localizes to the A band in the contracted state, suggesting that LMOD3 and KLHL40 dynamically colocalize. A recent study of the consequences of morpholino-mediated knockdown of Lmod3 in zebrafish also showed Lmod3 localizing at the A line, near the pointed end of the thin filament (10). While further characterization of LMOD3 localization is needed, it can be presently inferred that LMOD3 dynamically localizes along the A line to promote actin nucleation and thin filament elongation.

It is intriguing that mice lacking either KLHL40 or LMOD3 do not display cardiac abnormalities, despite high levels of expression of these proteins in the heart. It is conceivable that abnormalities in cardiac sarcomere function might manifest later in life, after the skeletal muscle defects cause lethality. Alternatively, other kelch domain and LMOD proteins expressed in the heart might substitute for the functions of KLHL40 and LMOD3. Future studies will address these questions.

Therapeutic implications. The realization that the absence of KLHL40 and LMOD3 causes nemaline myopathy and our delineation of the regulatory circuits that control the expression of these muscle-specific proteins raise interesting therapeutic possibilities for the future. For example, since KLHL40 stabilizes LMOD3, pharmacologic modulation of the degradation pathway through which KLHL40 controls the stability of LMOD3 would be expected to provide therapeutic benefit in nemaline myopathy. Moreover, the knowledge that KLHL40 and LMOD3 modulate MRTF/SRF and MEF2 signaling raises possibilities for therapeutically enhancing these transcriptional pathways via the protein kinases and G proteins that are known to regulate these transcription factors (19–22). Further delineation of the role of leiomodins and kelch domain proteins in muscle function and the transcriptional circuits they act within will help advance our understanding of nemaline myopathy and expand the therapeutic options for this lethal muscle disease.

Methods

Generation of mouse lines. *Lmod3*-KO mice were generated using TALEN mutagenesis as previously described (38–41). The Golden Gate TALEN Kit 2.0 was used to assemble 2 different TALEN pairs targeting the *Lmod3* locus, which were designed using the TAL Effector Nucleotide Targeter 2.0 (42, 43). Cleavage activity of TALENs was confirmed by using a cell-free in vitro cutting assay as previously described (ref. 39 and see the Supplemental Methods for additional details). TALE pairs were microinjected into fertilized oocytes collected from B6C3F1 superovulated females mated with B6C3F1 males as previously described (44, 45), then these eggs were implanted into pseudopregnant ICR females. Founders were analyzed for deleterious mutations using a T7 endonuclease assay as previously described (46). Two separate founders harboring Δ2 and Δ10 frameshift deletions, respectively, were crossed back to C57Bl/6 mice. Heterozygous intercrosses were conducted between mice harboring the same deletion in order to generate the KO mice. A detailed description of the targeting strategy, assembly, genotyping strategy, and primer sequences is provided in the Supplemental Methods.

MCK-Lmod3 mice were generated as previously described by placing the murine *Lmod3* coding sequence under the control of a 4.8-kb fragment of the muscle CK promoter and deriving Tg mice on a B6C3F1 background (47–49). For rescue experiments, *MCK-Lmod3* mice were intercrossed with *Lmod3* heterozygous mice (hereafter referred to as *HET* mice). The resulting *MCK-Lmod3*–KO mice were then crossed with *HET* mice to generate *MCK-LMOD3*–KO mice. All analyses were performed within the same mixed line using littermates as controls.

In order to generate *Lmod3-hsp68-LacZ* mice, different fragments of the *Lmod3* enhancer were subcloned into the *hsp68-LacZ* vector to make reporter constructs. Prepared transgenes were then injected into fertilized oocytes from B6C3F1 mice as previously described (30, 50), followed by oocyte transfer into pseudopregnant ICR mice. Embryos were then collected from the dams at designated time points.

RNA expression. RNA levels were analyzed using qPCR, Northern blotting and ISH, as previously described (51, 52). A complete list of the primers and probe sequences is provided in the Supplemental Methods.

Protein expression analysis in skeletal muscle. All immunoblotting experiments were performed using protein extracted from gastrocnemius muscle with anti-LMOD3 (14948-1-AP; Proteintech) and anti-GAPDH (MAB374; EMD Millipore) primary antibodies, followed by the appropriate HRP-conjugated secondary antibodies (Bio-Rad). See the Supplemental Methods for additional details.

Histology and immunohistochemistry. Skeletal muscle tissues were flash-frozen in a cryoprotective 3:1 mixture of tissue-freezing medium (Triangle BioSciences International) and gum tragacanth (Sigma-Aldrich) as previously described, followed by sectioning on a cryostat (31). Hearts and diaphragms were fixed in 4% paraformaldehyde, followed by paraffin embedding and sectioning as previously described. Routine H&E staining was performed on both paraffin-embedded tissue and cryosections as previously described (53). Desmin (M0760, clone D33; Dako) and laminin (L9393; Sigma-Aldrich) staining was performed on cryosections of skeletal muscle tissue as previously described (31, 54). Phalloidin staining was performed using rhodamine-conjugated phalloidin (R415; Molecular Probes, Life Technologies) on 5-μm-thick longitudinal skeletal muscle sections, which were fixed overnight and embedded in paraffin as previously described (6). Imaging of H&E-stained slides was done on a Leica DM2000 upright scope, and imaging of immunostained slides was done by confocal microscopy using a Zeiss LSM 700 microscope. Myofiber sizes were calculated using ImageJ software (NIH) for area threshold and particle analysis.

Electron microscopy. Samples were prepared for electron microscopy as previously described (55), and images were acquired using a FEI Tecnai G2 Spirit electron microscope equipped with an LaB_6 source Gatan CCD camera and operated at 120 kV.

Plasmid constructs. DNA fragments from the promoter region of LMOD3 were isolated by PCR using mouse genomic DNA as a template and cloned into a *LacZ* gene or the luciferase reporter pGL3 (Promega). Mutagenesis of MEF2 and SRF sites was performed using the QuikChange II Site-Directed Mutagenesis Kit (Agilent Technologies) according to the manufacturer's instructions. The pCDNA3.1 His/Myc-based MRTF-A, LMOD3, and KLHL40 expression vectors were previously reported (6, 18). SM22-4x-CArG and 3X-MEF2 luciferase reporter constructs were also previously reported (17, 18, 32). Primer sequences and plasmid construct designs are described in the Supplemental Methods.

Cell culture, transfection, and luciferase reporter assays. COS-7 cells (CRL-1651; ATCC) were grown in DMEM containing 10% FBS. Transfections were performed with FuGENE 6 Transfection Reagent (Promega) according to the manufacturer's instructions. For luciferase assays, cells were plated into 24-well dishes. After approximately 12 hours of incubation, transfection reagent was added. Unless indicated otherwise, 400 ng total plasmid DNA was used. A CMV promoter–driven *LacZ* expression plasmid was included for all transfections as an internal control (40 ng unless otherwise indicated). The total amount of each plasmid DNA per condition was kept constant by adding expression vectors without a cDNA insert if necessary. Twenty-four to thirty-six hours later, cells were lysed, and luciferase activity (Promega) and β-galactosidase (Invitrogen) activity were assessed according to the manufacturer's instructions. All experiments were performed in triplicate and were repeated at least twice.

Statistics. All data are presented as the mean value or percentage change ± SEM. Comparisons between 2 data sets were made using the Mann-Whitney *U* test for nonparametric data sets and the 2-tailed Student's *t* test for parametric data sets. The Kruskal-Wallis test was used for analysis of multiple groups, and Dunn's post test was used for pairwise comparisons. A *P* value of less than 0.05 was considered statistically significant.

Study approval. All experimental procedures involving animals in this study were reviewed and approved by the IACUC of the University of Texas Southwestern Medical Center.

Acknowledgments

We thank Rebecca Jackson, Robyn Leidel, Phoebe Doss, Anza Darehshouri, and Kate Luby-Phelps of the UT Southwestern Electron Microscopy Core Facility for their assistance and advice. We are grateful to José Cabrera for assistance with graphics. This work was supported by grants from the NIH (HL-077439, HL-111665, HL-093039, DK-099653, and U01-HL-100401); the Fondation Leducq Networks of Excellence; the Cancer Prevention and Research Institute of Texas; and the Robert A. Welch Foundation (1-0025, to E.N. Olson). N. Liu is supported by a Beginning Grant-in-Aid (BGIA) from the American Heart Association (AHA) (13BGIA17150004). B.K. Cenik is supported by the T32 NIH Pharmacological Sciences training grant (5T32GM007062-40).

Address correspondence to: Ning Liu or Eric N. Olson, Department of Molecular Biology, 5323 Harry Hines Blvd., Dallas, Texas 75390-9148, USA. Phone: 214.648.1187; E-mail: ning.liu@utsouthwestern.edu (N. Liu), E-mail: eric.olson@utsouthwestern.edu (E.N. Olson).

1. Ryan MM, et al. Clinical course correlates poorly with muscle pathology in nemaline myopathy. *Neurology*. 2003;60(4):665–673.
2. Romero NB, Clarke NF. Congenital myopathies. *Handb Clin Neurol*. 2013;113:1321–1336.
3. Romero NB, Sandaradura SA, Clarke NF. Recent advances in nemaline myopathy. *Curr Opin Neurol*. 2013;26(5):519–526.
4. North KN, Ryan MM. Nemaline Myopathy. *GeneReviews*. Seattle, Washington, USA: University of Washington; 2002.
5. Nowak KJ, Ravenscroft G, Laing NG. Skeletal muscle alpha-actin diseases (actinopathies): pathology and mechanisms. *Acta Neuropathol*. 2013;125(1):19–32.
6. Garg A, et al. KLHL40 deficiency destabilizes thin filament proteins and promotes nemaline myopathy. *J Clin Invest*. 2014;124(8):3529–3539.
7. Ravenscroft G, et al. Mutations in KLHL40 are a frequent cause of severe autosomal-recessive nemaline myopathy. *Am J Hum Genet*. 2013;93(1):6–18.
8. Marttila M, et al. Nebulin interactions with actin and tropomyosin are altered by disease-causing mutations. *Skelet Muscle*. 2014;4:15.
9. Gupta VA, Beggs AH. Kelch proteins: emerging roles in skeletal muscle development and diseases. *Skelet Muscle*. 2014;4:11.
10. Yuen M, et al. Leiomodin-3 dysfunction results in thin filament disorganization nemaline myopathy. *J Clin Invest*. 2014;124(11):4693–4708.
11. Nworu CU, Kraft R, Schnurr DC, Gregorio CC, Krieg PA. Leiomodin 3 Tropomodulin 4 have overlapping functions during skeletal myofibrillogenesis. *J Cell Sci*. 2015;128(2):239–250.
12. Campellone KG, Welch MD. A nucleator arms race: cellular control of actin assembly. *Nat Rev Mol Cell Biol*. 2010;11(4):237–251.
13. Chereau D, et al. Leiomodin is an actin filament nucleator in muscle cells. *Science*. 2008;320(5873):239–243.
14. Conley CA, Fritz-Six KL, Almenar-Queralt A, Fowler VM. Leiomodins: larger members of the tropomodulin (Tmod) gene family. *Genomics*. 2001;73(2):127–139.
15. Tsukada T, et al. Leiomodin-2 is an antagonist of tropomodulin-1 at the pointed end of the thin filaments in cardiac muscle. *J Cell Sci*. 2010;

123(pt 18):3136–3145.
16. Qualmann B, Kessels MM. New players in actin polymerization — WH2-domain-containing actin nucleators. *Trends Cell Biol*. 2009;19(6):276–285.
17. Wang DZ, et al. Potentiation of serum response factor activity by a family of myocardin-related transcription factors. *Proc Natl Acad Sci U S A*. 2002;99(23):14855–14860.
18. Kuwahara K, Barrientos T, Pipes GC, Li S, Olson EN. Muscle-specific signaling mechanism that links actin dynamics to serum response factor. *Mol Cell Biol*. 2005;25(8):3173–3181.
19. Olson EN, Nordheim A. Linking actin dynamics and gene transcription to drive cellular motile functions. *Nat Rev Mol Cell Biol*. 2010;11(5):353–365.
20. Miralles F, Posern G, Zaromytidou AI, Treisman R. Actin dynamics control SRF activity by regulation of its coactivator MAL. *Cell*. 2003;113(3):329–342.
21. Vartiainen MK, Guettler S, Larijani B, Treisman R. Nuclear actin regulates dynamic subcellular localization and activity of the SRF cofactor MAL. *Science*. 2007;316(5832):1749–1752.
22. Miano JM, Long X, Fujiwara K. Serum response factor: master regulator of the actin cytoskeleton and contractile apparatus. *Am J Physiol Cell Physiol*. 2007;292(1):C70–C81.
23. Potthoff MJ, Olson EN. MEF2: a central regulator of diverse developmental programs. *Development*. 2007;134(23):4131–4140.
24. Esnault C, et al. Rho-actin signaling to the MRTF coactivators dominates the immediate transcriptional response to serum in fibroblasts. *Genes Dev*. 2014;28(9):943–958.
25. Schnell C, Kan A, North KN. 'An artefact gone awry': identification of the first case of nemaline myopathy by Dr R.D.K. Reye. *Neuromuscul Disord*. 2000;10(4–5):307–312.
26. Ilkovski B, et al. Nemaline myopathy caused by mutations in the muscle α-skeletal-actin gene. *Am J Hum Genet*. 2001;68(6):1333–1343.
27. Grayson J, Williams RS, Yu YT, Bassel-Duby R. Synergistic interactions between heterologous upstream activation elements and specific TATA sequences in a muscle-specific promoter. *Mol Cell Biol*. 1995;15(4):1870–1878.
28. Leibham D, et al. Binding of TFIID and MEF2 to the TATA element activates transcription of the Xenopus MyoDa promoter. *Mol Cell Biol*. 1994;14(1):686–699.
29. He A, Kong SW, Ma Q, Pu WT. Co-occupancy by multiple cardiac transcription factors identifies transcriptional enhancers active in heart. *Proc Natl Acad Sci U S A*. 2011;108(14):5632–5637.
30. Kothary R, et al. Inducible expression of an hsp68-lacZ hybrid gene in transgenic mice. *Development*. 1989;105(4):707–714.
31. Liu N, et al. Requirement of MEF2A, C, and D for skeletal muscle regeneration. *Proc Natl Acad Sci U S A*. 2014;111(11):4109–4114.
32. Kuwahara K, et al. Modulation of adverse cardiac remodeling by STARS, a mediator of MEF2 signaling and SRF activity. *J Clin Invest*. 2007;117(5):1324–1334.
33. Malfatti E, et al. Muscle histopathology in nebulin-related nemaline myopathy: ultrastrastructural findings correlated to disease severity and genotype. *Acta Neuropathol Commun*. 2014;2:44.
34. Carlier MF, et al. Structure, function, and evolution of the β-thymosin/WH2 (WASP-Homology2) actin-binding module. *Ann N Y Acad Sci*. 2007;1112:67–75.
35. Paunola E, Mattila PK, Lappalainen P. WH2 domain: a small, versatile adapter for actin monomers. *FEBS Lett*. 2002;513(1):92–97.
36. Rasson AS, Bois JS, Pham DS, Yoo H, Quinlan ME. Filament assembly by spire: key residues and concerted actin binding. *J Mol Biol*. 2015;427(4):824–839.
37. DiFranco M, Quinonez M, Capote J, Vergara J. DNA transfection of mammalian skeletal muscles using in vivo electroporation. *J Vis Exp*. 2009;(32):e1520.
38. Miller JC, et al. A TALE nuclease architecture for efficient genome editing. *Nat Biotechnol*. 2011;29(2):143–148.
39. Bedell VM, et al. In vivo genome editing using a high-efficiency TALEN system. *Nature*. 2012;491(7422):114–118.
40. Kato T, et al. Production of Sry knockout mouse using TALEN via oocyte injection. *Sci Rep*. 2013;3:3136.
41. Sung YH, Jin Y, Kim S, Lee HW. Generation of knockout mice using engineered nucleases. *Methods*. 2014;69(1):85–93.
42. Cermak T, et al. Efficient design and assembly of custom TALEN and other TAL effector-based constructs for DNA targeting. *Nucleic Acids Res*. 2011;39(12):e82.
43. Doyle EL, et al. TAL Effector-Nucleotide Targeter (TALE-NT) 2.0: tools for TAL effector design and target prediction. *Nucleic Acids Res*. 2012;40(Web Server issue):W117–W122.
44. Long C, et al. Prevention of muscular dystrophy in mice by CRISPR/Cas9-mediated editing of germline DNA. *Science*. 2014;345(6201):1184–1188.
45. Wang H, et al. One-step generation of mice carrying mutations in multiple genes by CRISPR/Cas-mediated genome engineering. *Cell*. 2013;153(4):910–918.
46. Kim HJ, Lee HJ, Kim H, Cho SW, Kim JS. Targeted genome editing in human cells with zinc finger nucleases constructed via modular assembly. *Genome Res*. 2009;19(7):1279–1288.
47. Kim MS, et al. Protein kinase D1 stimulates MEF2 activity in skeletal muscle and enhances muscle performance. *Mol Cell Biol*. 2008;28(11):3600–3609.
48. Naya FJ, et al. Stimulation of slow skeletal muscle fiber gene expression by calcineurin in vivo. *J Biol Chem*. 2000;275(7):4545–4548.
49. Sternberg EA, et al. Identification of upstream and intragenic regulatory elements that confer cell-type-restricted and differentiation-specific expression on the muscle creatine kinase gene. *Mol Cell Biol*. 1988;8(7):2896–2909.
50. Cheng TC, Hanley TA, Mudd J, Merlie JP, Olson EN. Mapping of myogenin transcription during embryogenesis using transgenes linked to the myogenin control region. *J Cell Biol*. 1992;119(6):1649–1656.
51. Hargrave M, Koopman P. In situ hybridization of whole-mount embryos. *Methods Mol Biol*. 2000;123:279–289.
52. Millay DP, et al. Myomaker is a membrane activator of myoblast fusion and muscle formation. *Nature*. 2013;499(7458):301–305.
53. Wu H, et al. Regulation of mitochondrial biogenesis in skeletal muscle by CaMK. *Science*. 2002;296(5566):349–352.
54. Liu N, et al. Mice lacking microRNA 133a develop dynamin 2-dependent centronuclear myopathy. *J Clin Invest*. 2011;121(8):3258–3268.
55. Nelson BR, et al. Skeletal muscle-specific T-tubule protein STAC3 mediates voltage-induced Ca^{2+} release and contractility. *Proc Natl Acad Sci U S A*. 2013;110(29):11881–11886.